Mitigation Method of the Shaft Voltage According to Parasitic Capacitance of the PMSM

Jun-kyu Park, Thusitha Randima Wellawatta, Sung-Jin Choi, and Jin Hur, *Senior Member, IEEE*

***Abstract*—This study proposes the shaft voltage mitigation method according to change in parasitic capacitances of a permanent magnet synchronous motor. To consider the shaft voltage reduction in the initial motor design process without any filter, the parasitic capacitances affecting the shaft voltage are calculated using the motor geometry parameters. Then, the shaft voltage is analyzed according to change in parasitic capacitances using the equivalent circuit model and the torque characteristic is also analyzed to effectively mitigate the shaft voltage. As a result, the rotor-to-winding is determined as an appropriate parameter to mitigate the shaft voltage among the parasitic capacitances, because it affects the shaft voltage and does not affect the output torque. Finally, the shaft voltage mitigation method according to variation of rotor-to-winding capacitance is verified by experiment.**

***Index Terms*—Bearing current, common-mode voltage (CMV), equivalent circuit, parasitic capacitance, permanent magnet synchronous motor (PMSM), shaft voltage.**

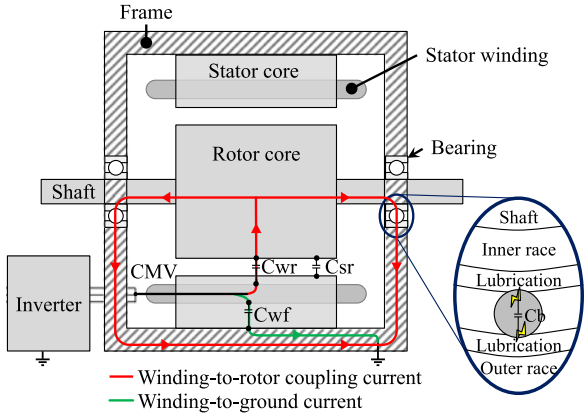

Fig. 1. System overview.

I. Introduction

PERMANENT magnet synchronous motors (PMSMs) driven by a space vector pulse-width modulation (SVPWM) inverter are widely used in lots of industrial fields due to their high power density and high torque. In the drive system, however, they have the major cause of motor bearing failure due to fast switching of the SVPWM [1]–[3]. Practically, all SVPWM inverters generate a common-mode voltage (CMV) relative to the ground, which creates a shaft voltage through parasitic capacitances of the motor [4]–[7].

The electric field of the stator winding allows us many parasitic capacitance couplings in excrescent places. The high dv/dt in the CMV excites these capacitance links. The results of this connection generate a voltage in rotor shaft. This concept was mentioned in [5]–[8]. Specifically, bearings are connected in two different paths. One is connected in parallel with the air–gap capacitor (capacitance between the stator and the rotor, defined as Csr), and another is connected in series with the parasitic capacitance between the winding and rotor (Cwr). Generally, bearing current by high dv/dt is not considered as risk factor because it is very small [8], [9]. However, if the effective bearing impedance becomes small due to electric discharge machining (EDM) effect (The electric breakdown field strength of the lubricant is at approximately 10–15 V/μm [8], [10]), bearing races and balls become short because EDM effect causes the dielectric breakdown of the lubricant film, as shown in Fig. 1. For this reason, the shaft voltage is discharged as a shaft current through the bearing.

Owing to increase in the maintenance and downtime costs, attention on protecting the motor bearing has increased. Thus, lots of studies have been conducted on the shaft voltage reduction [11]–[17]. In [11], microfiber ring is applied as a basic solution. It grounded the shaft voltage directly, but it also needs to be replaced after degrading. In [12], a slot wedge based reduction method was proposed to mitigate shaft to ground voltage. In [13], an insulated hybrid bearing concept was proposed. The bearing is made by nonconductive materials for this technique but it limits the mechanical strength of the motor. In addition, slot-embedded partial electrostatic shield concept was proposed in [14] to reduce the capacitive coupling between the stator windings and the rotor. On the inverter side, lots of studies have conducted on the reduction of the CMV [15]–[17]. As a disadvantage of previous studies, those reduction methods require additional installations or nonconductive materials.

Manuscript received February 11, 2017; revised May 1, 2017; accepted May 2, 2017. Date of publication June 19, 2017; date of current version September 18, 2017. Paper 2016-EMC-1436.R1, presented at the 2016 IEEE Energy Conversion Congress and Exposition, Milwaukee, WI, USA, Sep. 18–22, and approved for publication in the IEEE Transactions on Industry Applications by the Electric Machines Committee of the IEEE Industry Applications Society. This work was supported by a Incheon National University (International Cooperative) Research Grant in 2016. *(Corresponding Author: Jin Hur.)*

J. K. Park and J. Hur are with the Department of Electrical Engineering, Incheon National University, Incheon 406-772, South Korea (e-mail: porpoise17@nate.com; jinhur@inu.ac.kr).

T. R. Wellawatta and S. J. Choi are with the School of Electrical Engineering, University of Ulsan, Ulsan 680-749, South Korea (e-mail: trwellawatta@gmail.com; sjchoi@ulsan.ac.kr).

Color versions of one or more of the figures in this paper are available online at http://ieeexplore.ieee.org.

Digital Object Identifier 10.1109/TIA.2017.2717378

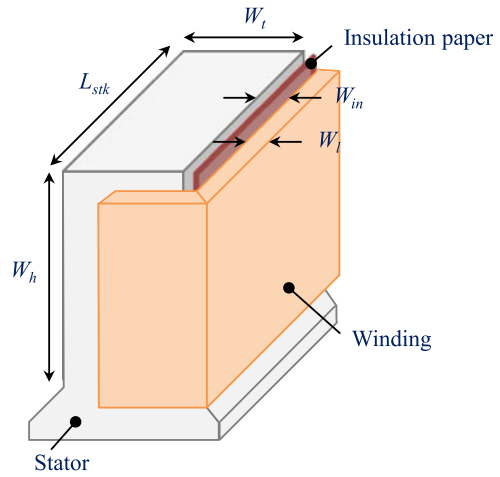

Fig. 2. Structure of the stator and the winding.

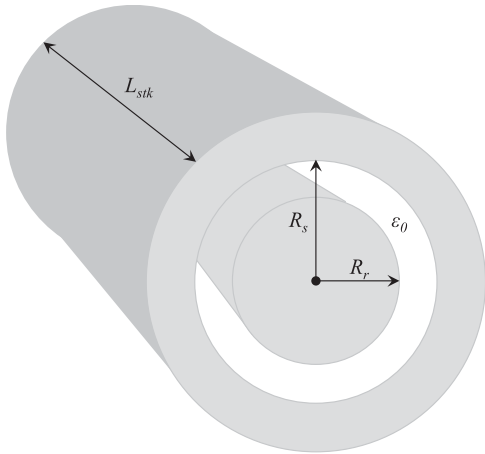

Fig. 3. Configuration of the stator and the rotor.

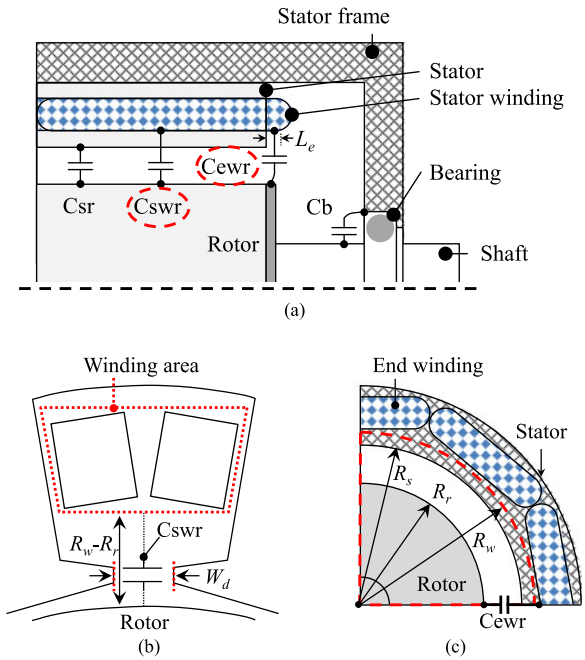

Fig. 4. Configuration of the stator winding and the rotor. (a) Mechanism of occurrence of Cwr. (b) Stator winding-to-rotor (Cswr). (c) End winding-to-rotor (Cewr).

In this study, a shaft voltage mitigation method is proposed by changing parasitic capacitances that can be considered in motor initial design process. Thus, parasitic capacitances coupled with winding, stator, and rotor are calculated using motor design parameters, and shaft voltage is analyzed using equivalent circuit model according to change in the effective parasitic capacitances. As a result, rotor-to-winding capacitance is determined as a variable parameter through the analysis of the correlation between the parasitic capacitances and output torque characteristics because rotor-to-winding capacitance has greatest effect on the shaft voltage and has no effect on the average torque. Finally, shaft voltage mitigation method according to change in winding-to-rotor capacitance (Cwr) is verified by experiment.

II. Analysis of Parasitic Capacitances and Shaft Voltage

The CMV causes the shaft voltage and provides bearing current through the parasitic capacitive coupling between the winding, the stator, and the rotor [4]–[6]. Thus, parasitic capacitances need to be calculated using motor geometry parameters in order to consider the reduction of the shaft voltage in initial motor design process. Basically, capacitance can be obtained by simple equation as follows:

$$C = \varepsilon_0 \varepsilon_r \frac{A}{d} \tag{1}$$

where C is the capacitance, ε_0 is the permittivity of air, ε_r is the relative static permittivity (or dielectric constant), A is the cross-section area of the conductive plate, and d is the distance between two conductive plates (or thickness of dielectric).

In the electric field, winding, stator, and rotor can be considered as conductive plates. For this reason, the shaft voltage is charged by those parasitic capacitive coupling. Thus, parasitic capacitances existing in the motor can be calculated based on the geometry of the motor.

A. Winding-to-Stator Capacitance (Cws)

Cws is the capacitance between the winding and the stator. The cross sections of the winding facing the stator and the cross sections of stators facing the winding can act as parallel conductive plates, and insulation paper can act as dielectric, as shown in Fig. 2. The windings surround the four sides of the stator. Thus, the equation of the Cws is classified into two parts as follows:

$$\mathrm{Cws} = \frac{S}{3}\varepsilon_0\varepsilon_{\mathrm{in}}\left(\frac{2(W_h \times L_{\mathrm{stk}})}{W_{\mathrm{in}}} + \frac{2(W_h \times W_t)}{W_{\mathrm{in}}}\right) \tag{2}$$

where S is the number of the slots, W_h is the coil height that lay on the stator, W_l is the width of the coil from the coil side, W_t is the width of the stator teeth, W_{in} is the width of the insulation paper, $\varepsilon_{\mathrm{in}}$ is the permittivity of the insulation, and L_{stk} is the stack length of stator.

B. Stator-to-Rotor Capacitance (Csr)

Csr is the capacitance existing between the stator and the rotor. If the slot opening is neglected, the stator and the rotor

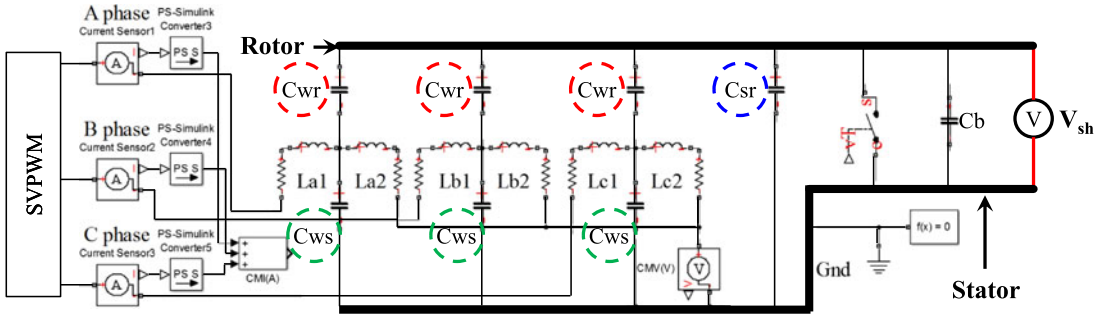

Fig. 5. Equivalent circuit model consisting of parasitic capacitances.

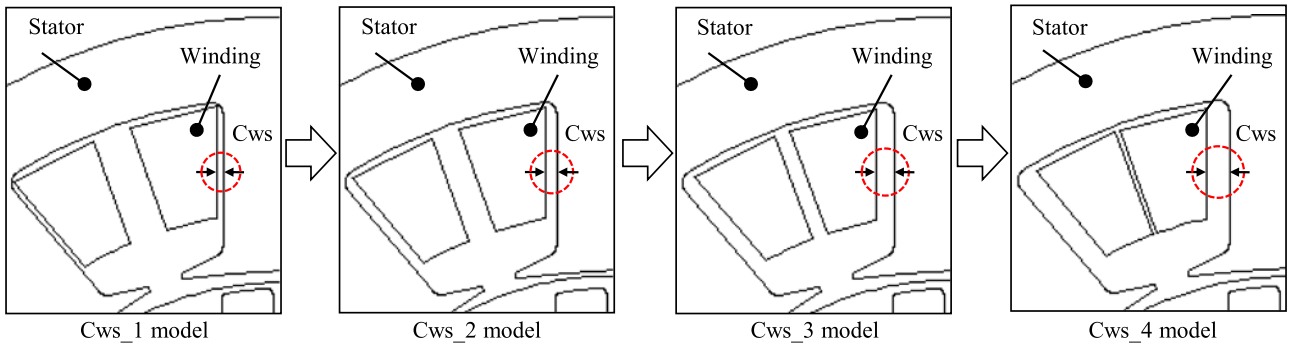

Fig. 6. Different type of models according to change in Cws.

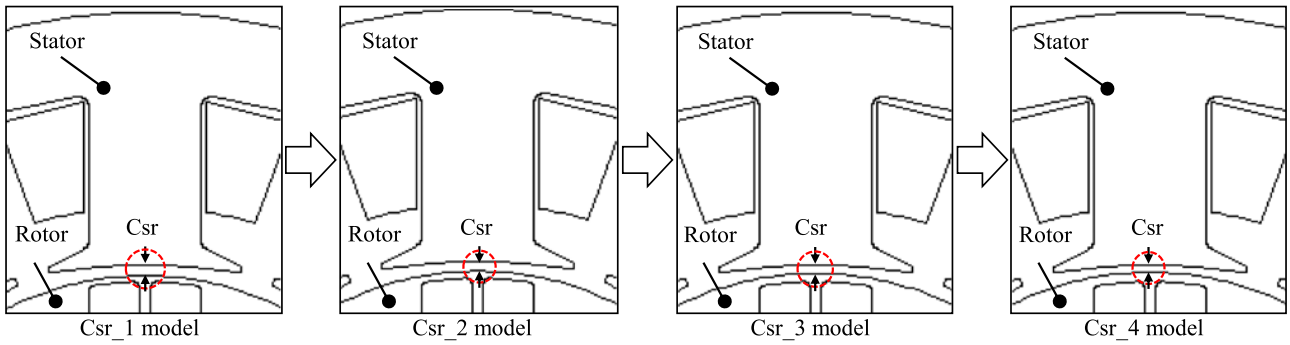

Fig. 7. Different type of models according to change in Csr.

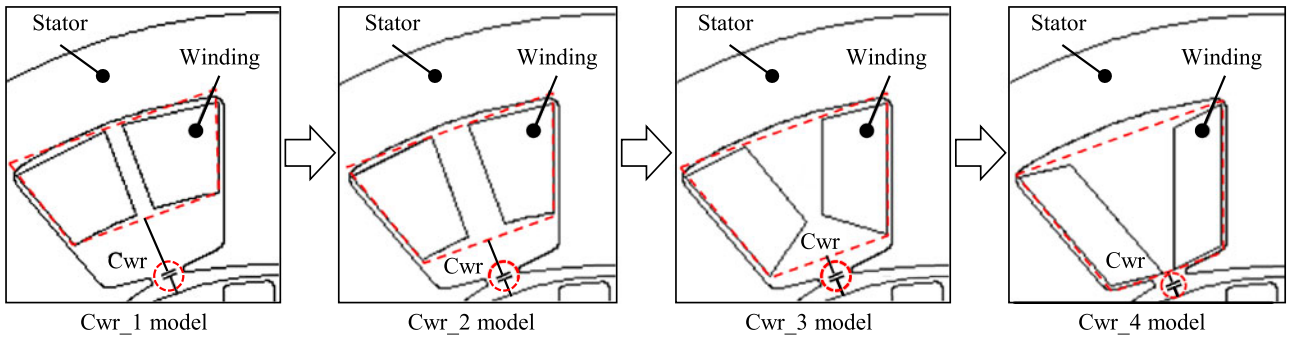

Fig. 8. Different type of models according to change in Cwr.

TABLE I
MOTOR GEOMETRY PARAMETERS ACCORDING TO VARIATION OF WINDING-TO-STATOR CAPACITANCE (ε_0: 8.8419$*10^{-12}$, $\varepsilon_{\rm in}$: 3)

Item	$R_{\rm r}$ (mm)	$R_{\rm r}$ (mm)	$R_{\rm w}$ (mm)	$W_{\rm d}$ (mm)	$W_{\rm h}$ (mm)	$W_{\rm l}$ (mm)	$W_{\rm in}$ (mm)	H (mm)	$L_{\rm stk}$ (mm)	$L_{\rm e}$ (mm)	S
Cws_1	28	27	32.7	3	12	6.5	0.5	8.28	52.6	6	9
Cws_2	28	27	32.7	3	12	6.5	1.0	9.77	52.6	6	9
Cws_3	28	27	32.7	3	12	6.5	1.5	10.87	52.6	6	9
Cws_4	28	27	32.7	3	12	6.5	2.0	13.16	52.6	6	9

TABLE II
MOTOR GEOMETRY PARAMETERS ACCORDING TO VARIATION OF STATOR-TO-ROTOR CAPACITANCE

Item	$R_{\rm r}$ (mm)	$R_{\rm r}$ (mm)	$R_{\rm w}$ (mm)	$W_{\rm d}$ (mm)	$W_{\rm h}$ (mm)	$W_{\rm l}$ (mm)	$W_{\rm in}$ (mm)	H (mm)	$L_{\rm stk}$ (mm)	$L_{\rm e}$ (mm)	S
Csr_1	28	27	32.7	3	12	6.5	0.5	8.28	52.6	6	9
Csr_2	28	27.1	32.7	3	12	6.5	0.5	9.77	52.6	6	9
Csr_3	28	27.2	32.7	3	12	6.5	0.5	10.87	52.6	6	9
Csr_4	28	27.3	32.7	3	12	6.5	0.5	13.16	52.6	6	9

TABLE III
MOTOR GEOMETRY PARAMETERS ACCORDING TO VARIATION OF WINDING-TO-ROTOR CAPACITANCE

Item	$R_{\rm r}$ (mm)	$R_{\rm r}$ (mm)	$R_{\rm w}$ (mm)	$W_{\rm d}$ (mm)	$W_{\rm h}$ (mm)	$W_{\rm l}$ (mm)	$W_{\rm in}$ (mm)	H (mm)	$L_{\rm stk}$ (mm)	$L_{\rm e}$ (mm)	S
Cwr_1	28	27	34.2	3	7.79	8.93	0.5	8.28	52.6	6	9
Cwr_2	28	27	32.7	3	9.3	7.19	0.5	9.77	52.6	6	9
Cwr_3	28	27	31.6	3	10.39	7.19	0.5	10.87	52.6	6	9
Cwr_4	28	27	29.3	3	11.91	4.65	0.5	13.16	52.6	6	9

can be assumed as a concentric cylindrical capacitor, as shown in Fig. 3. Thus, the inner cross section of the stator and the outer cross section of the rotor can act as conductive plates, and it depends on an air-gap length. Finally, Csr can be calculated as

$$\mathrm{Csr} = \frac{2\pi\varepsilon_0 L_{\rm stk}}{\ln\frac{R_s}{R_r}} \tag{3}$$

where R_s is the stator inner radius and R_r is the rotor outer radius.

C. Winding-to-Rotor Capacitance (Cwr)

Cwr is the parasitic capacitance existing between the winding and the rotor. In the study, Cwr is classified into two parts taking into account the stator winding and end winding parts such as stator winding-to-rotor (Cswr) and end winding-to-rotor (Cewr), as shown in Fig. 4.

In case of the Cswr, the cross section of the rotor and bottom surface of the winding facing the rotor can act as the electrode of the parallel plate capacitor, as shown in Fig. 4(b). In addition, the gap between the rotor and the winding can be a distance of the plates. In the study, slot opening area is determined as effective cross section of the plates because the slot opening creates the area of the capacitor. Thus, Cswr can be calculated as (4).

In case of the Cewr, it is difficult to consider practical shape of the end winding. Thus, the end winding is assumed as a concentric cylindrical capacitor, as shown in Fig. 4(c). Thus, Cewr can be calculated as (5), and finally total Cwr can be obtained by summing Cswr and Cewr,

$$\mathrm{Cswr} = \frac{\frac{S}{3}\varepsilon_0 W_d L_{\rm stk}}{R_w - R_r} \tag{4}$$

$$\mathrm{Cewr} = \frac{4\pi\varepsilon_0 L_e}{3\ln\frac{R_s+R_w}{2R_r}} \tag{5}$$

where W_d is the width of the slot opening, L_e is the thickness of the end winding from the stator, and R_w is the radius of the stator and end windings.

D. Shaft Voltage ($V_{\rm sh}$)

Fig. 5 shows the equivalent circuit model, which is proposed in [18], in order to calculate the shaft voltage. The equivalent circuit is controlled by SVPWM and main parameters of the equivalent circuit are Cws, Csr, and Cwr. Based on the equivalent circuit, shaft voltage ($V_{\rm sh}$) can be simply calculated as in (6) and CMV is generally calculated by average value of three phase voltages as in (7). Finally, it denotes that shaft voltage is proportional to the CMV and Cwr, and inversely proportional to the Csr and the Cb,

$$V_{\rm sh} = \frac{\mathrm{CMV}}{\frac{\mathrm{Csr}+Cb}{3\mathrm{Cwr}}+1} \tag{6}$$

$$\mathrm{CMV} = \frac{V_{a,\rm gnd}+V_{b,\rm gnd}+V_{c,\rm gnd}}{3}. \tag{7}$$

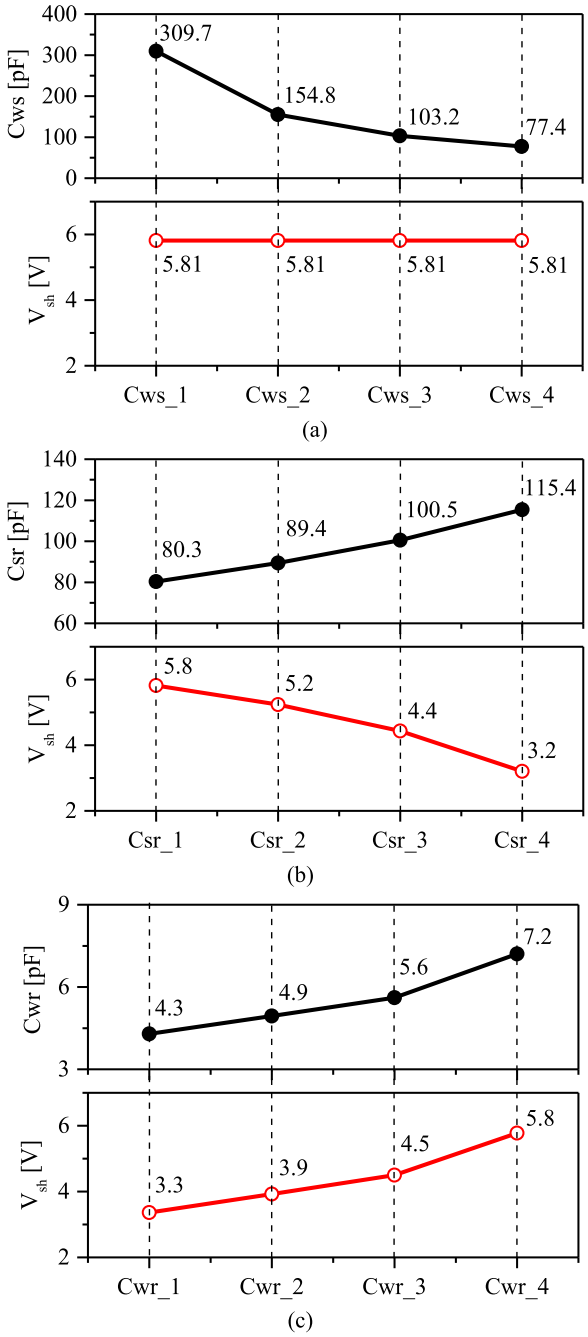

Fig. 9. Variation of the V_{sh}. (a) According to variation of Cws. (b) According to variation of Csr. (c) According to variation of Cwr.

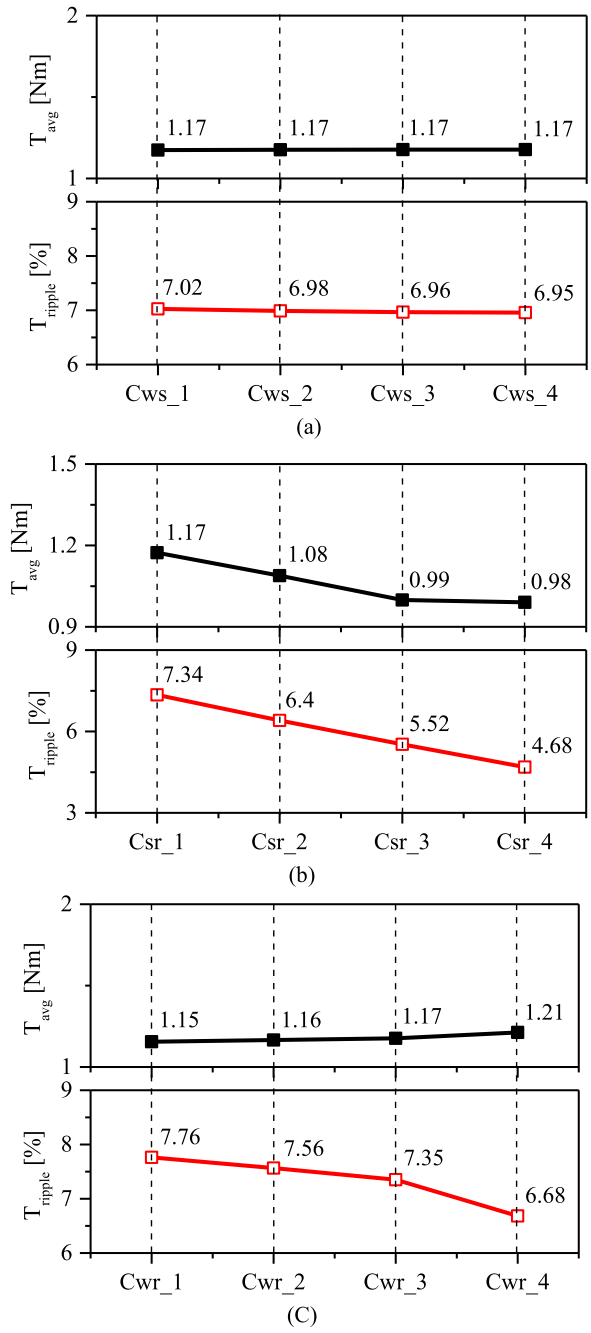

Fig. 10. Variation of the T_{avg} and T_{ripple}. (a) According to variation of Cws. (b) According to variation of Csr. (c) According to variation of Cwr.

III. Modifying Concept of Parasitic Capacitances

Based on the analysis of the parasitic capacitances, three types of models are demonstrated and compared according to change in the parasitic capacitances. In the motor, there are several parasitic capacitances but representative parasitic capacitances (Cws, Csr, and Cwr) are considered in the paper. In case of the ball bearing capacitance (Cb), it is a critical component for the shaft voltage. However, Cb is not considered as a mitigation parameter because standard of industrial bearings is fixed according to size.

Figs. 6–8 show the different models according to parasitic capacitance types in order to determine the appropriate models for reducing the shaft voltage. The variation of parasitic capacitances is implemented by modifying the winding shape with following considerations.

1) All models maintain the number of windings and the fill factor (ratio of winding area per slot area).
2) Cws model assumes that distance between the winding and the stator depends on the insulation paper or plastic thickness.
3) Csr models are designed by changing the rotor diameter while maintaining the winding shape.

4) Cwr models are designed by changing the distance between the winding and the rotor while maintaining the rotor diameter in order to maintain the air-gap length.

Fig. 6 shows the four types of models according to the changes in Cws. The distance between the stator and the winding was changed by increasing the insulator thickness. The insulation thickness of Cws_1, Cws_2, Cws_3, and Cws_4 is, respectively, determined as 0.5, 1.0, 1.5, and 2.0 mm, as shown in Table I. Here W_h is kept the constant value in order to confirm the shaft voltage by only change in the Cws without change in the Cwr.

Fig. 7 shows the four types of models according to changes in Csr. The variations in the Csr are implemented by changing the rotor diameter while keeping the inner diameter of the stator. The rotor diameter of Csr_1, Csr_2, Csr_3, and Csr_4 is, respectively, determined as 27, 27.1, 27.2, and 27.3 mm, as shown in Table II.

Fig. 8 shows the different types of models according to changes in Cwr. The variations of Cwr are implemented by modifying the winding shape without change in the air-gap length. In addition, distance between the winding and the stator should keep the constant value in order to confirm the shaft voltage by changing the Cwr with a little change in the Cws. The variation of motor geometry is represented in Table III.

IV. Results and Discussion

A. Analysis of Shaft Voltage and Torque Characteristics Due to Variation of Cws, Csr, and Cwr

Fig. 9 shows the variation in $V_{\rm sh}$ according to changes in Cws, Csr, and Cwr. The results of $V_{\rm sh}$ are obtained by equivalent circuit model using the SIMULINK. Furthermore, Fig. 10 shows the variation in the average torque $(T_{\rm avg})$ and torque ripple $(T_{\rm ripple})$ according to change in the Cws, Csr, and Cwr. The torque characteristics are obtained by finite element method (FEM) simulation using the ANSYS MAXWELL. The comparison analysis of the torque characteristics ($T_{\rm avg}$ and $T_{\rm ripple}$) and parasitic capacitances is considered to determine the appropriate parasitic capacitance for mitigating the shaft voltage in the initial motor design process.

Fig. 9(a) shows the relationship between $V_{\rm sh}$ and Cws. Here it is confirmed that Cws does not much related to the $V_{\rm sh}$ because $V_{\rm sh}$ maintains constant value according to change in Cws. Specifically, Cws is directly connected to the ground, so that most energized voltage in Cws does not affect the shaft. In addition, it is also confirmed that Cws does not also affect the torque characteristics because there is no variation of the torque characteristics according to change in Cws, as shown in Fig. 10(a). In practice, increasing the distance between the winding and the stator causes the increase in the winding resistance. For this reason, input current needs to be increased a little in order to satisfy the rated torque. However, it does not significantly affect the torque characteristics because the variation of winding inductance is adequate to accommodate a little increase in the input current.

Fig. 9(b) and (c) shows the relationship between $V_{\rm sh}$ and Csr, and $\rm V_{sh}$ and Cwr, respectively. Here $\rm V_{sh}$ is not only reduced as increases in Csr but also increased as decreases in Cwr. For this reason, it is confirmed that Csr and Cwr are significantly affect the shaft voltage.

However, Csr causes the reduction of the average torque $(T_{\rm avg})$ because increasing the Csr increases the air-gap length, as shown in Fig. 10(b). Basically, an air-gap magnetic flux density, which is main factor of the output torque, depends on the air-gap length. For this reason, it is determined that Csr is not appropriate parameter to reduce the shaft voltage in initial motor design process. On the other hand, $T_{\rm avg}$ maintains constant value according to change in the Cwr, as shown in Fig. 10(c). Therefore, it is determined that the Cwr is appropriate parameter for reducing the shaft voltage because decreasing the Cwr reduces the shaft voltage and does not affect torque characteristics.

TABLE IV
Specifications And Dimensions of IPMSM

Components	Item	Unit	Value
Input & output Characteristics	Input voltage	$V_{\rm dc}$	60
	Rated power	W	400
	Rated torque	N · m	1.1
	Rated speed	rpm	3500
Winding	No. of windings per phase	–	72
	Fill factor	%	32
Structure & Dimensions	No. of poles	–	6
	No. of slots	–	9
	Stator outer diameter	mm	100
	Stator inner diameter	mm	56
	Rotor outer diameter	mm	54
	Air-gap length	mm	1
	Stack length	mm	52.6
Bearing (6202Z/ 6201Z)	Bearing ball radius	mm	2.975
	Radius of clearance with ball	mm	2.985
	No. of bearing balls	-	8/ 7
	Permittivity of lubricant	-	2
Inverter	Switching frequency	kHz	20

TABLE V
Parasitic Capacitances

Item	Calculated Value (pF)	Measured Value (pF)	Error (%)
Cws	156.449	149.8	3.27
Cwr	7.506	7.1	5.41
Csr	87.850	90.5	2.92
Cb (6202Z, 6201Z)	–	65.7	–

B. Simulation and Experimental Results According to Variation of Cwr

In the study, 6-pole 9-slot IPMSM is used in the simulation and the experiment. The specifications and dimensions of the motor are represented in the Table IV. In addition, the comparison of calculated and measured parasitic capacitances is represented in Table V in order to verify (2)–(5). The motor geometry parameters, in Tables I–III, are used for calculating the parasitic capacitances Cws, Cwr, and Csr. In case of the Cb, measured value is used in simulation.

Fig. 11(a) shows the experimental model with normal Cwr (Cwr_n), and Fig. 11(b) shows the experimental model with

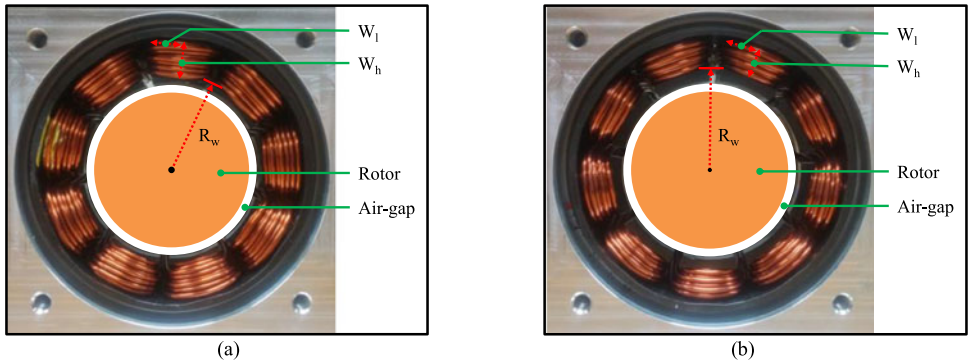

Fig. 11. Experimental models according to different Cwr values. (a) Cwr_n model. (b) Cwr_m model.

TABLE VI
MOTOR GEOMETRY PARAMETERS ACCORDING TO CWR_N AND CWR_M

Item		R_s (mm)	R_r (mm)	R_w (mm)	W_d (mm)	W_h (mm)	W_l (mm)	L_{stk} (mm)	L_e (mm)	S
Cwr_n	Simulation	28	27	29.3	3	11.91	4.65	52.6	6	9
	Experiment	28	27	30.1	3	12	4.7	52.6	6	9
Cwr_m	Simulation	28	27	34.2	3	7.79	8.93	52.6	6	9
	Experiment	28	27	34.5	3	7.9	8.9	52.6	6	9

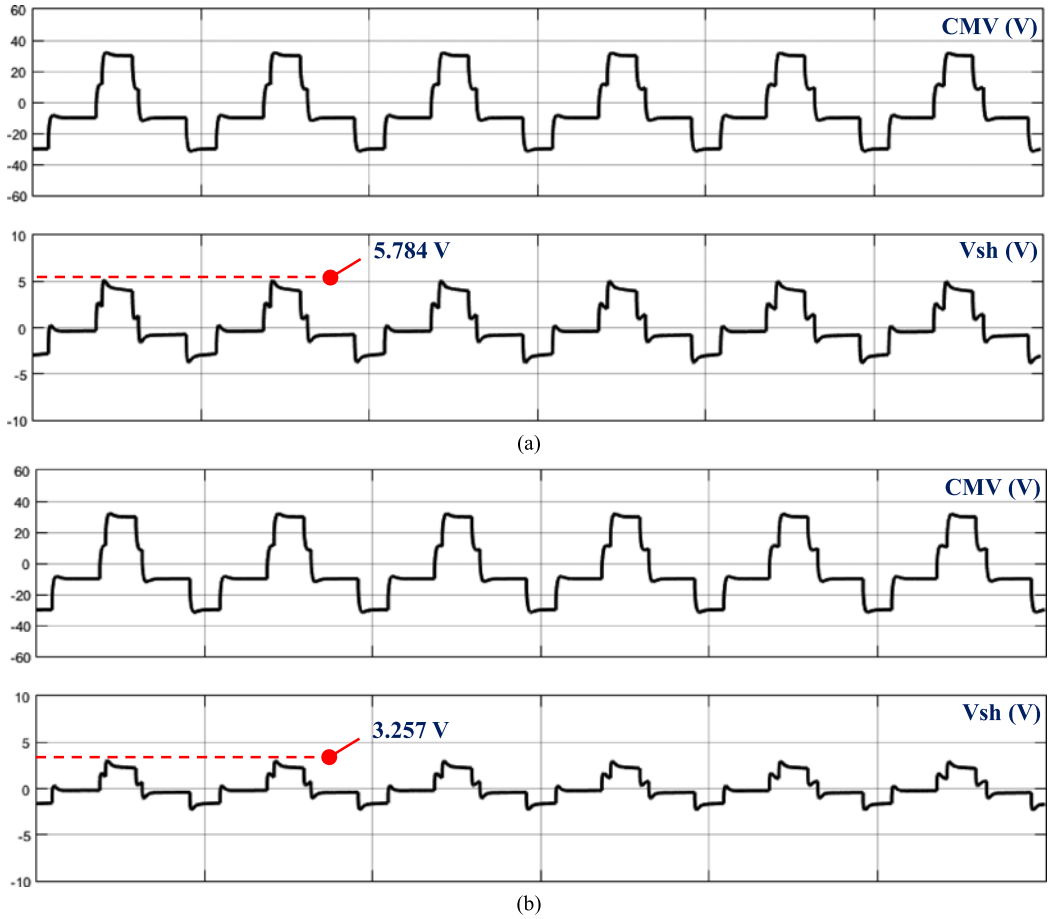

Fig. 12. Simulation results of CMV and V_{sh}. (a) Cws_n model. (b) Cws_m model.

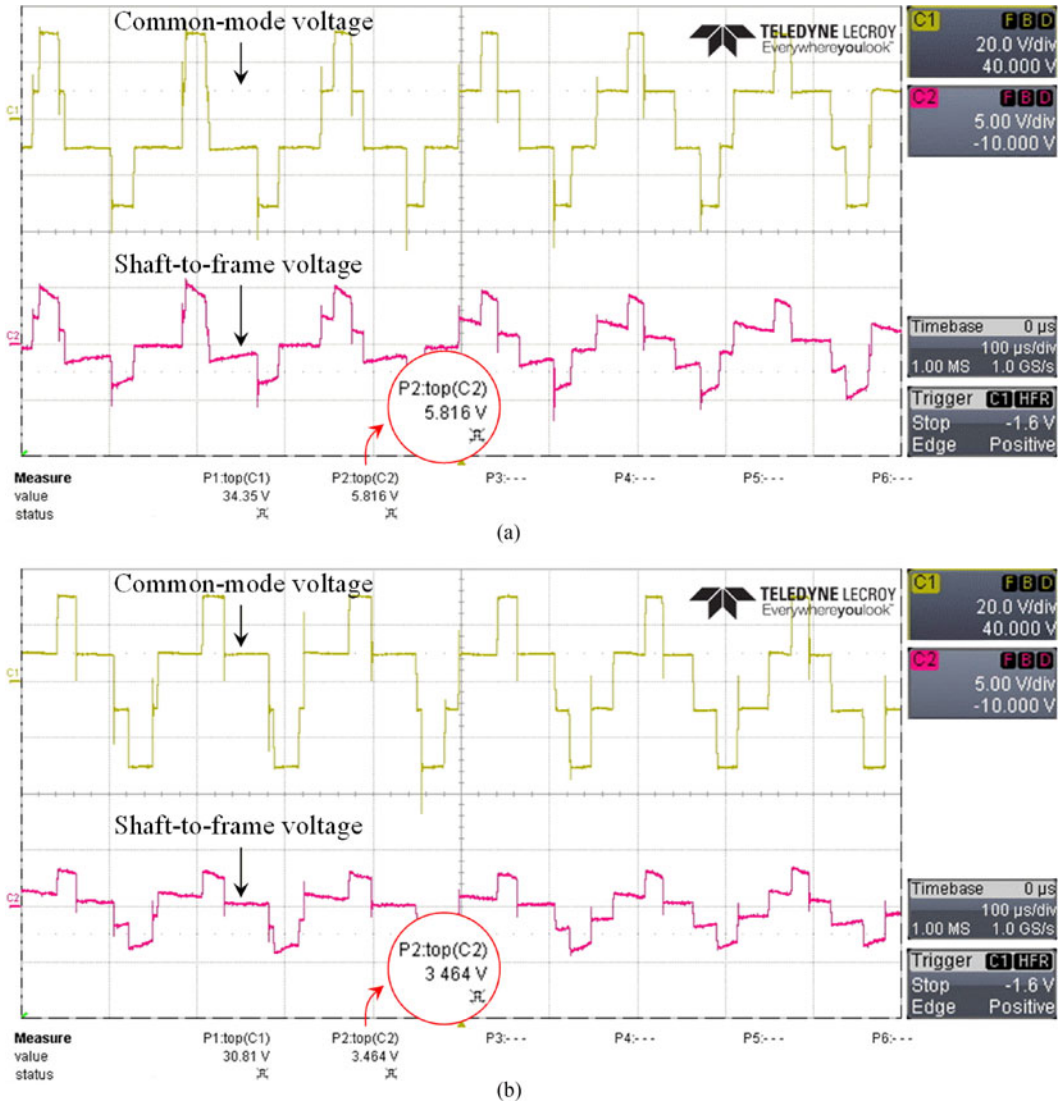

Fig. 13. Experimental results. (a) With normal winding configuration. (b) With modified winding configuration.

modified Cwr (Cwr_m). In the study, Cwr_m is implemented by modifying the winding shape. The windings are wounded by shifting towards the outside of the stator, as shown in Fig. 11(b). Table IV represents the motor geometry parameters for calculating Cwr, according to different winding shapes. Basically, the two different models have same inner stator diameter and outer rotor diameter in order to prevent the variation of the Csr and have same thickness insulation paper in order to prevent the variation of the Cws.

Table VI represents the motor geometry parameters according to Cwr_n and Cwr_m used in the simulation and the experimental models. The motor geometry parameters of the experimental model is designed almost the same with that of the simulation model. Fig. 12 shows the simulation results of the CMV and the $V_{\rm sh}$, for the Cwr_n and Cwr_m models. As a result, $V_{\rm sh}$ is reduced from 5.784 to 3.257 V. In addition, Fig. 13 shows the experimental results of the CMV and the $V_{\rm sh}$. As a result, $V_{\rm sh}$ is reduced up to 3.464 V from 5.816 V.

V. Conclusion

This paper proposes the shaft voltage mitigation method without additional filter, according to change in parasitic capacitances. First, parasitic capacitances are analyzed and calculated by using motor geometry parameters. Then, shaft voltage and output torque characteristics are, respectively, analyzed by equivalent circuit model and FEM simulation tool, ANSYS MAXWELL. As a result, it is confirmed that the Cws does not affect both the shaft voltage and the torque characteristics. On the other hand, Csr and Cwr affect the shaft voltage. In addition, Csr affects the torque characteristics because Csr depends on the air-gap length. Otherwise, the influence of Cwr on the torque characteristics is very insignificant, compared with that of Csr. Thus, Cwr is determined as an appropriate parasitic capacitance for reducing the shaft voltage. Based on the analysis of the parasitic capacitances, Cwr is modified by biasing the windings towards the outside of the stator and this method. Actually, the proposed method is limited by the slot fill factor

because the proposed method is implemented by changing the winding configuration. It means that the machine with high slot fill factor is more difficult to reduce Cwr than machine with low slot fill factor. However, there is possibility that the proposed method can reduce the shaft voltage. In this study, the machine with 32% slot fill factor is used for implementing the simulation and the experiment. As a result, shaft voltage is reduces up to 3.257 V from 5.784 V when the proposed method is applied to this machine.

Therefore, modifying winding shape can mitigate the shaft voltage.

REFERENCES

[1] S. S. Kwak and S. K. Mun, "Model predictive control methods to reduce common-mode voltage for three-phase voltage source inverters," *IEEE Trans. Power Electron.*, vol. 30, no. 9, pp. 5019–5035, Sep. 2015.

[2] T, Maetani, S. Morimoto, K. Yamamoto, Y. Isomura, and A. Watanabe, "Comparing brushless DC motors: A method of suppressing the shaft voltage even in a grounded motor frame," *IEEE Ind. Appl. Mag.*, vol. 21, no. 6, pp. 29–35, Nov./Dec. 2015.

[3] J. K. Park, T. Wellawatta, S. J. Choi, and J. Hur, "Mitigation method of the shaft voltage according to parasitic capacitance of the PMSM," in *Proc. 2016 IEEE Energy Convers. Congr. Expo.*, Milwaukee, WI, USA, 2016, pp. 1–6. doi:10.1109/ECCE.2016.7855245.

[4] J. Adabi, F. Zare, A. Ghosh, and R. D. Lorenz, "Calculations of capacitive coupling in induction generators to analyse shaft voltage," *IEEE Trans. IET Power Electron.*, vol. 3, no. 3, pp. 379–390, May 2010.

[5] J. Adabi, A. A. Boora, F. Zare, A. Nami, A. Ghosh, and F. Blaabjerg, "Common-mode voltage reduction in a motor drive system with a power factor correction," *IET Power Electron*., vol. 5, no. 3, pp. 366–375, 2012.

[6] S. Chen, T. A. Lipo, and D. Fitzgerald, "Modeling of motor bearing currents in PWM inverter drives," *IEEE Trans. Ind. Appl.*, vol. 32, no. 6, pp. 1365–1370, Nov./Dec. 1996.

[7] S. Chen, T. A. Lipo, and D. Fitzgerald, "Source of induction motor bearing currents caused by PWM inverters" *IEEE Trans. Energy Convers.*, vol. 11, no. 1, pp. 25–32, Mar. 1996.

[8] D. Busse, J. Erdman, R. J. Kerkman, D. Schlegel, and G. Skibinski, "System electrical parameters and their effects on bearing currents," *IEEE Trans. Ind. Appl.*, vol. 33, no. 2, pp. 577–584, Mar./Apr. 1997.

[9] H. Akagi and S. Tamura, "A passive EMI filter for eliminating both bearing current and ground leakage current from an inverter-driven motor," *IEEE Trans. Power Electron.*, vol. 21, no. 5, pp. 1459–1469, Sep. 2006.

[10] M. J. Costello, "Shaft voltage and rotating machinery," *IEEE Trans. Ind. Appl.*, vol. 29, no. 2, pp. 1615–1625, Jun. 1993.

[11] A. Muetze and H. W. Oh, "Design aspects of conductive microfiber rings for shaft-grounding purposes," *IEEE Trans. Ind. Electron.*, vol. 44, no. 6, pp. 1749–1757, Apr. 2008.

[12] B. Bai, Y. Wang, and X. Wang, "Suppression for discharging bearing current in variable-frequency motors based on electromagnetic shielding slot wedge," *IEEE Trans. Magn.*, vol. 51, no. 11, Nov. 2015, Art. no. 8109404.

[13] A. Muetze and A. Binder, "Don't lose your bearings," *IEEE Ind. Appl. Mag.*, vol. 12, no. 4, pp. 22–31, Jul/Aug. 2006.

[14] F. J. T. E. Ferreira, M. V. Cisteleca, and A. T. de Almeida, "Evaluation of slot-embedded partial electrostatic shield for high-frequency bearing current mitigation in inverter-fed induction motors," *IEEE Trans. Energy Convers.*, vol. 27, no. 2, pp. 382–390, Jun. 2012.

[15] J. Kalaiselvi and S. Srinivas, "Bearing currents and shaft voltage reduction in dual-inverter-fed open-end winding induction motor with reduced CMV PWM methods," *IEEE Trans. Ind. Electron.*, vol. 62, no. 1, pp. 144–152, Jan. 2015.

[16] H. Akagi and T. Doumoto, "An approach to eliminating high-frequency shaft voltage and ground leakage current from an inverter-driven motor," *IEEE Trans. Ind. Appl.*, vol. 40, no. 4, pp. 1162–1169, Jul./Aug. 2004.

[17] M. C. D. Piazza, A. Ragusa, and G. Vitale, "Effect of common-mode active filtering in induction motor drives for electric vehicles," *IEEE Trans. Veh. Technol.*, vol. 59, no. 6, pp. 2664–2673, Jul. 2010.

[18] J. K. Park, T. R. Wellawatta, Z. Ullah, and J. Hur, "New equivalent circuit of IPM-type BLDC motor for calculation of shaft voltage by considering electric and magnetic fields," *IEEE Trans. Ind. Appl.*, vol. 52, no. 5, pp. 3763–3771, Sep./Oct. 2016.

Jun-Kyu Park was born in Busan, South Korea, in 1986. He received the B.S., M.S., and Ph.D. degrees in electrical engineering from the University of Ulsan, Ulsan, South Korea, in 2011, 2013, and 2017, respectively.

Since March 2017, he has been a Lecturer with the Department of Electrical Engineering, Incheon National University, Incheon, South Korea. His current research interests include the motor design, motor vibration analysis, and fault diagnosis of the motor.

Thusitha Randima Wellawatta was born in Colombo, Sri Lanka, in 1985. He received the B.S. degree in electrical engineering from the Engineering Council, London, U.K., in 2012, and has been working toward the Ph.D. degree in electrical engineering with the University of Ulsan, Ulsan, South Korea, since 2014.

His research interests include dc–dc converters, maximum power point tracking systems, and coupling problem analysis.

Sung-Jin Choi received the B.S., M.S., and Ph.D. degrees in electrical engineering from Seoul National University, Seoul, South Korea, in 1996, 1998, and 2006, respectively.

From 2006 to 2008, he was a Research Engineer at Palabs Company, Ltd., Seoul. From 2008 to 2011, he was at Samsung Electronics Company, Ltd., Suwon, South Korea, as a Senior and Principal Research Engineer developing LED drive circuits and wireless battery charging system. In 2011, he joined the University of Ulsan, Ulsan, South Korea, where he is currently an Associate Professor with the School of Electrical Engineering. His research interests include component modeling, topology and control of high frequency switching converters, and power electronics for renewable energy sources.

Jin Hur (SM'03) received the Ph.D. degree in electrical engineering from Hanyang University, Seoul, South Korea, in 1999.

From 1999 to 2000, he was in the Department of Electric Engineering, Texas A&M University, College Station, TX, USA, as a Postdoctoral Research Associate. From 2000 to 2001, he was a Research Professor of electrical engineering for BK21 projects at Hanyang University, Seoul. From 2002 to 2007, he was a Director of the Intelligent Mechatronics Research Center, Korea Electronics Technology Institute, Puchon, South Korea, where he worked on the development of special electric machines and systems. From 2008 to August, 2015, he was an Associate Professor with the School of Electric Engineering, University of Ulsan, Ulsan, South Korea. Since August 2015, he has been a Professor with the Department of Electrical Engineering, Incheon National University, Incheon, South Korea. He is the author of more than 180 publications on electric machine design, analysis and control, and power electronics. He has one granted pending U.S. patent and 20 granted pending Korean patents. His current research interests include high-performance electrical machines, modeling, drives, and new concept actuators for special purposes and numerical analysis of electromagnetic fields.

Prof. Hur is an Associate Editor for IEEE TRANSACTION ON POWER ELECTRONICS.